HHS Public Access

Author manuscript

FASEB J. Author manuscript; available in PMC 2022 September 01.

Published in final edited form as:

FASEB J. 2021 September ; 35(9): e21862. doi:10.1096/fj.202100883R.

Metformin and leucine increase satellite cells and collagen remodeling during disuse and recovery in aged muscle

Jonathan J. Petrocelli[1], **Ziad S. Mahmassani**[1], **Dennis K. Fix**[1], **Jessie A. Montgomery**[2], **Paul T. Reidy**[3], **Alec I. McKenzie**[4], **Naomi M. de Hart**[5], **Patrick J. Ferrara**[6], **Joshua J. Kelley**[1], **Hiroaki Eshima**[5], **Katsuhiko Funai**[1,5,6], **Micah J. Drummond**[1,6]

[1]Unviersity of Utah, Department of Physical Therapy & Athletic Training, Salt Lake City, UT, USA

[2]University of Utah, Department of Chemistry, Salt Lake City, UT, USA

[3]Miami University, Department of Kinesiology, Nutrition and Health, Oxford, OH, USA

[4]University of Utah, Department of Internal Medicine, Salt Lake City, UT, USA

[5]University of Utah, Department of Nutrition and Integrative Physiology, Salt Lake City, UT, USA

[6]University of Utah, Molecular Medicine Program, Salt Lake City, UT, USA

Abstract

Loss of muscle mass and strength after disuse followed by impaired muscle recovery commonly occurs with aging. Metformin and leucine individually have shown positive effects in skeletal muscle during atrophy conditions but have not been evaluated in combination nor tested as a remedy to enhance muscle recovery following disuse atrophy in aging. The purpose of this study was to determine if a dual treatment of metformin and leucine (MET+LEU) would prevent disuse-induced atrophy and/or promote muscle recovery in aged mice and if these muscle responses correspond to changes in satellite cells and collagen remodeling. Aged mice (22–24 mo) underwent 14 days of hindlimb unloading (HU) followed by 7 or 14 days of reloading (7 or 14d RL). Metformin (MET), leucine (LEU), or MET+LEU was administered via drinking water and were compared to Vehicle (standard drinking water) and Ambulatory baseline (AMB). We observed that during HU, MET+LEU resolved whole body grip strength and soleus muscle specific force decrements caused by HU. Gastrocnemius satellite cell abundance was increased with MET+LEU treatment but did not alter muscle size during disuse or recovery conditions. Moreover, MET+LEU treatment alleviated gastrocnemius collagen accumulation caused by HU and increased collagen turnover during 7 and 14d RL driven by a decrease in collagen IV content. Transcriptional pathway analysis revealed that MET+LEU altered muscle hallmark pathways related to inflammation and myogenesis during HU. Together, the dual treatment of metformin

Address for correspondence: Micah J. Drummond, Ph.D., University of Utah, Department of Physical Therapy & Athletic Training, 520 Wakara Way, Salt Lake City, UT, 84108-1213, Phone: (801) 585-1310, Fax: (801) 585-5629, micah.drummond@hsc.utah.edu.

Author Contributions

J.J. Petrocelli and M.J. Drummond designed the research; J.J. Petrocelli, Z.S. Mahmassani, D.K. Fix, and H. Eshima performed the research; J.J. Petrocelli, Z.S. Mahmassani, J.A. Montgomery, P.J. Ferrara conducted data analyses. P.T. Reidy, A.I. McKenzie, N.M. de Hart, P.J. Ferrara, and J.J. Kelley contributed to data collection; K. Funai contributed reagents and analytical tools. J.J. Petrocelli and M.J. Drummond wrote the manuscript. All authors contributed to editing the manuscript.

Conflict of Interest

The authors report no conflicts of interest.

and leucine was able to increase muscle function, satellite cell content, and reduce collagen accumulation, thus improving muscle quality during disuse and recovery in aging.

Keywords

Fibrosis; inflammation; hindlimb unloading; reloading; aging; extracellular matrix

Introduction

Periods of skeletal muscle disuse in older adults are followed by impaired muscle size and function recovery [1]. Other than exercise, there is not a consistent clinically adopted approach to enhance the recovery of muscle following disuse in aging. Although beneficial, exercise does not always fully recover muscle mass and strength losses in elderly individuals [2] while many older adults needing muscle rehabilitation are not able to partake in exercise programs or achieve optimal exercise intensity due to pain or logistical barriers [3]. Therefore, advancements in pharmacological and nutritional approaches are needed to prevent disuse atrophy and enhance muscle recovery following disuse in aging.

Metformin, a first line therapy to treat type 2 diabetes mellitus, has gained interest in aging research due to possible alternate usage to prevent/delay age-related diseases. In rodents, metformin has demonstrated promise to improve skeletal muscle outcomes in response to atrophic stimuli yet appears to blunt muscle adaptations to exercise in humans [4]. However, metformin has shown to prevent cardiotoxin-induced muscle damage [5], promoted muscle mass recovery from burn injury [6], and prevented muscle mass loss and muscle fibrosis due to limb immobilization [7] thus alluding to metformin being uniquely beneficial during tissue damage or atrophy. Mechanistically, metformin activates AMP-activated protein kinase (AMPKα) and PPARG coactivator-1alpha (PGC-1α) in skeletal muscle tissues and cells [8, 9]. It is believed that metformin activation of these pathways could promote improved muscle recovery since overexpression of PGC-1α in skeletal muscle was capable of alleviating inflammatory signaling and atrophy in young mice [10].

Similarly, leucine, a branched-chain amino acid, may also promote improved recovery as it is well established to stimulate muscle protein synthesis and reduce breakdown through activation of mechanistic target of rapamycin complex 1 (mTORC1) [11]. In aged rat skeletal muscle, a leucine-supplemented diet reduced protein breakdown in the post-prandial state [12] and leucine, when supplemented with antioxidants, promoted protein synthesis and accelerated muscle mass recovery following immobilization in adult rats [13]. The use of leucine alone to prevent disuse atrophy in rodents and humans has displayed mixed results [14, 15]. Thus, it is possible that leucine combination therapies may be more beneficial to promote positive outcomes to overcome disuse muscle atrophy and promote recovery in aging.

Combination therapies could be a promising approach to enhance outcomes in skeletal muscle capitalizing on unique pathways that are dysregulated in the organism or offering synergy. For instance, metformin and vitamin D combined therapy reduced muscle fibrosis and improved hyperglycemia in diabetic rats [16]. In another study, metformin when

combined with leucine induced synergistic effects to enhanced skeletal muscle insulin sensitivity [17]. While mechanistic studies are lacking, it is believed that metformin and leucine combination synergize on the SIRT1-AMPKα-PGC-1α signaling cascade to improve protein turnover, increase mitochondrial function and promote muscle mass and strength [18]. However, it is unclear if leucine and metformin when combined have further beneficial effects on aging muscle and regrowth conditions.

Muscle regrowth and regeneration involve a complex interplay of multiple cell types including muscle progenitor stem cells (satellite cells) that ultimately lead to restoration of the extracellular matrix (ECM) and resolution of muscle size and function. The primary ECM defect in skeletal muscle results from excessive collagen accumulation, known as muscle fibrosis. Muscle fibrosis alters myofibril mechanical properties leading to impaired contractility and contributes to reductions in satellite cell content [19]. Metformin and leucine individually have exhibited an ability to increase satellite cell content and proliferation [6, 20]. Satellite cells are required for muscle regeneration following injury [21], and coordinate with fibroblasts and the ECM to regulate muscle fibrosis and ECM remodeling events [21, 22]. Excessive muscle fibrosis is frequently observed in aging muscle [23], associated with poor muscle regeneration, and is a common occurrence in muscle during disuse in rodents [24]. Of interest, metformin was effective to reduce muscle fibrosis following high fat feeding [25] and limb immobilization [7] in rodents while, in another study, leucine prevented muscle collagen accumulation following cryogenic injury [26]. However, the use of metformin or metformin combination therapies, such as with leucine, to enhance satellite cells or prevent fibrosis in aging as a mechanism to improve muscle and functional recovery is unknown.

Therefore, the purpose of this study was to identify if metformin combined with leucine treatment could prevent disuse atrophy and/or enhance muscle recovery (muscle size and function) in aged mice and if this is paralleled with changes in satellite cell content and muscle fibrosis. We hypothesized that the combination of metformin and leucine would enhance satellite cells, reduce fibrosis, and these changes would promote muscle recovery (size and function) following disuse in aged mice.

Methods

Animals and Metformin and Leucine Administration

Male C57BL/6 mice aged 22–24 months acquired from the National Institute on Aging were housed with ad libitum access to food (standard chow) and water and maintained on a 12-hour light/dark cycle. Mice (n=8–12/group were administered metformin (MET), leucine (LEU), or metformin and leucine combination (MET+LEU) treatments via drinking water. Vehicle-treated control mice received drinking water absent of the above treatments. Leucine and MET+LEU in drinking water was prepared fresh every other day and metformin was prepared in drinking water prior to initiation of hindlimb unloading and again prior to reloading. Mice received an average metformin concentration of 336.6 mg/kg/d ± 7.5 SE (approximately a human equivalent of 2g/d), and an average leucine concentration of 2.3 g/kg/d ± 0.1 SE. Leucine concentration was based on a dose of 1.5 g leucine/100 mL drinking water which has demonstrated in mice to promote skeletal muscle mTORC1

signaling. Treatments did not alter water or food consumption as all mice had an average food intake of ~3.5 g/d ± 0.1 SE and water intake of ~4.6 mL/d ± 0.1 SE. All animal procedures were conducted in accordance with guidelines set by the University of Utah Institutional Animal Care and Use Committee and in accordance with the ethical standards laid down in the 1964 Declaration of Helsinki.

Hindlimb Unloading and Reloading

Mice were randomly assigned to the following experimental groups: Ambulatory baseline (AMB), 14 days of hindlimb unloading (HU), 7 days of reloading/re-ambulation following HU (7d RL), and 14 days of reloading following HU (14d RL) (Figure 1). These time points were chosen as our previous report displayed impaired recovery 7 days post HU in aged mice [27], and here we further characterized late recovery (14d RL) responses. Ambulatory baseline mice freely ambulated in a standard cage (2–4 animals/cage) and did not receive any treatments and did not undergo any intervention (HU or reloading). For HU, mice underwent a modified Morey-Holton hindlimb unloading design [28], with modifications [27, 29]. Two mice/cage were housed together during HU. Body weight, water and food intake were monitored to confirm no excessive weight loss due to malnutrition or dehydration. For reloading experiments, the HU apparatus was removed, and mice were given free access to ambulate while housed with the same mouse as during disuse (2 mice/cage). After experimentation, mice were fasted 4h then euthanized under isoflurane followed by cervical dislocation. Soleus and gastrocnemius muscles were rapidly dissected, weighed, and frozen in liquid nitrogen or OCT (Fisher Scientific, Waltham, MA, USA) in isopentane, and stored at −80°C. Gastrocnemius muscles were separated into red and white portions prior to storage. For protein and RNA collection, ~90% white gastrocnemius was used with ~10% red gastrocnemius as we have observed a fiber type distribution of ~90% fast twitch and ~10% slow twitch fibers in gastrocnemius.

Grip Strength

Whole body grip strength was assessed utilizing a grip strength meter with a mesh wire attachment (Columbus Instruments, Columbus, OH, USA). Mice would ambulate across the mesh wire briefly before being pulled by the base of their tail parallel to the mesh wire. Five trials were conducted, and peak force recorded. The average peak force of the five trials was assessed as whole body grip strength.

Muscle Force Production

In a separate group of mice from each group, the soleus muscle was dissected under anesthetization as described in [30] and analyzed for ex vivo muscle force production. In brief, soleus muscles were tied at each tendon into the horizontal bath tissue system from Aurora Scientific Inc. (Ontario, CA, Model: 400A) containing oxygenated Krebs-Ringer's solution supplemented with 8 mM glucose. The muscle was stimulated with a single pulse (20V, pulse width 0.2 ms) and stretched until optimal force-producing length was achieved. The muscle was then allowed to equilibrate for 5 min before being stimulated with frequencies ranging from 10 to 200 Hz (20V, pulse width 0.2 ms, 2 min between stimulations). Forces produced were recorded in real-time via a force transducer using Aurora Scientific Dynamic Muscle Control software (DMCv5.500) for data acquisition and

Dynamic Muscle Analysis software (DMAv5.321) for data analyses. The specific force was calculated using cross-sectional area (CSA) of the muscle tissue, which was estimated from the weight and length of the muscle (mN/mm^2).

Immunofluorescence and Histology

Frozen OCT-embedded soleus and gastrocnemius muscles were sectioned at 10μm on a cryo-stat. Whole soleus cross-sections were examined while gastrocnemius muscles were split in the sagittal plane. Sagittal gastrocnemius sections contained equal proportions of red and white fibers compared to whole gastrocnemius sections. Immunofluorescent stained slides were observed with a fully automated wide-field light microscope (Nikon Ti, Tokyo, Japan) with the X10 objective lens. Images were taken using a high sensitivity Andor Clara CCD camera (Belfast, UK). Sirius Red histology slides were imaged with a Zeiss Slide Scanner Axio Scan.Z1 (Carl Zeiss Inc., Oberkochen, GER) with the X20 objective lens.

To assess myofiber CSA and fiber type, muscle sections were blocked for 1h with mouse IgG blocker, M.O.M (Vector, San Diego, CA, USA cat# MKB-2213). Sections were then incubated in primary laminin antibody (1:200, Sigma, St. Louis, MO, USA, cat# L9393) and primary antibodies BA.D5, SC.71, and BF.F3 (1:100 Developmental Studies Hybridoma Bank, Univ. of Iowa) overnight in 4°C, followed by secondary antibody AMCA (Vector, San Diego, CA, USA Cat# Cl-1000) for laminin and Alexa Fluor 647, 555, and 488 for fiber types (Invitrogen, Carlsbad, CA, USA, cat# A21242, A21121, and A21426). CSA and fiber type was measured using semi-automatic muscle analysis with segmentation of histology, a MATLAB application (SMASH) [31], and confirmed with ImageJ software [32]. Using the SMASH software an average of 2,437 ± 73 SE gastrocnemius and 623 ± 76 SE soleus fibers were included in the CSA analysis for each muscle.

For satellite cell and central nuclei assessment, muscle sections were fixed in 4% paraformaldehyde, washed, and incubated in sodium citrate buffer at 92°C for 20 min and cooled to room temperature for antigen retrieval. Endogenous peroxidases were blocked with 3% H_2O_2 followed by 1h mouse IgG blocker, M.O.M (Vector, San Diego, CA, USA cat# MKB-2213). Muscles were incubated in primary pax7 antibody (1:100, Developmental Studies Hybridoma Bank, Univ. of Iowa) and laminin (1:200, Sigma, St. Louis, MO, USA, cat# L9393) overnight at 4°C. Secondary antibodies: biotinylated goat anti mouse IgG (Jackson ImmunoResearch, West Grove, PA, USA, cat# 115-065-205) and Alexa Fluor 488 (Invitrogen, Carlsbad, CA, USA, cat# A21042) were utilized for pax7 and laminin, respectively. The Tyramide SuperBoost Kit with Alexa Fluor 568 (Invitrogen, Carlsbad, CA, USA, cat# B40956) was used following the manufacturer's instructions to amplify pax7 signal. Slides were mounted with vector shield fluorescent mounting media containing DAPI (Vector, San Diego, CA, USA, cat# H-1200) to observe nuclei. Satellite cells were counted with ImageJ software and determined by co-occurrence with pax7 and DAPI staining. Central nuclei were counted as nuclei not incorporated in the fiber boarder. Using ImageJ software, an average of 457 ± 16 SE gastrocnemius and 726 ± 15 SE soleus fibers were counted in each muscle to determine satellite cells and central nuclei per fiber.

For immunoglobin G (IgG) analysis, muscle sections were fixed in cold acetone (−20°C), blocked with 5% BSA for 30 minutes and incubated in FITC-conjugated mouse anti-IgG

(1:100, Vector, San Diego, CA, USA, cat# FI-2000) overnight at 4°C. IgG was analyzed using Nikon Elements Advanced Research (Nikon, Tokyo, Japan) software to determine percent area stained. The area of IgG was determined based off per channel thresholds determined using ambulatory control, age-matched mice.

To assess collagen IV and biotinylated-collagen hybridizing peptide (B-CHP; degraded collagen) content, cross sections were fixed in cold (−20°C) acetone, blocked with streptavidin and biotin (Vector, San Diego, CA, USA, cat# SP-2001), and incubated in 15 μM B-CHP (3-Helix, Salt Lake City, UT, USA) following manufacturer instructions. Primary collagen IV antibody (Abcam, Cambridge, UK, cat# ab6586) was added with B-CHP and incubated for 1h at room temperature, followed by an overnight incubation at 4°C. Dylight 594 (1:200, Thermofisher, Waltham, MA, USA, cat# SA-5549) and secondary antibody Alexa Fluor 647 (Invitrogen, Carlsbad, CA, USA, cat# 21245) were utilized for B-CHP and collagen IV, respectively. B-CHP and collagen IV were analyzed using Nikon Elements Advanced Research (Nikon, Tokyo, Japan) software to determine percent area stained. The area of collagen IV and B-CHP was determined based off per channel thresholds determined using ambulatory control, age-matched mice.

For Sirius Red staining, muscle sections were fixed in Bouin's solution (Labchem, Zelienople, PA, USA, cat# LC117901) for 1h at 56°C. After washing, muscles were incubated in Picro Sirius Red solution (American MasterTech Scientific, Lodi, CA, USA, cat# STPSRPT) for 40 min at room temperature. Muscles were then rinsed in 0.5% glacial acetic acid, then dehydrated via incubation in 90, 95 and 100% ethanol for 20s each. The sections were then quickly dipped in xylene and mounted to glass cover slips using Cytoseal XYL (ThermoScientific, Waltham, MA, USA, cat# 83124). Sirius Red was analyzed using Nikon Elements Advanced Research software as described in [33]. Briefly, Sirius Red stained area percentage was determined using color thresholding and the area stained was outlined using region of interest tools. The threshold for Sirius Red was determined using ambulatory control, age-matched mice.

Immunoblotting

Proteins were isolated by homogenizing 50 mg gastrocnemius tissue in ice-cold lysis buffer (50 mM Tris-HCl pH 7,4m 150 mM NaCl, 1 mM PMSF, 1% Triton X-100, 0.5% sodium deoxycholate, 0.1% SDS, phosphatase inhibitor and protease inhibitor with EDTA (Roche)) using a pre-chilled glass tube and mechanically driven pestle. Lysates were centrifuged (10,000 rpm for 10 min at 4°C), and supernatant was collected. Protein concentrations were determined using a BCA assay (ThermoScientific, Waltham, MA, USA). Proteins were run through a 7.5% polyacrylamide gel electrophoresis and transferred onto a polyvinylidene difluoride membrane. Membranes were blocked 1h in 5% BSA-TSBT at room temperature, primary antibodies were used 1:1000 in 5% BSA-TBST overnight at 4°C, and secondary antibodies were mixed at 1:4000 in 2% non-fat dairy milk for 1h at room temperature. Membranes were incubated with ECL Prime Western Blotting Detection Reagent (GE Healthcare, Chicago, IL, USA, cat# RPN2236) and imaged using a ChemiDoc XRS (Bio-Rad, Hercules, CA, USA) and quantified with Image Lab Software (Bio-Rad, Hercules, CA, USA). The following primary antibodies were purchased from Cell Signaling Technologies

(Danvers, MA, USA): AMPK, cat# 2532; p-AMPK(Thr172), cat# 2531; ACC, cat# 3676; p-ACC(Ser79), cat# 11818; mTOR, cat# 2983; p-mTOR(Ser2448), cat# 2971; rpS6, cat# 2217; p-rpS6 (Ser240/244), cat# 2215; p70S6K, cat# 9202; p-p70S6K(Thr389), cat# 9205. PGC-1α primary antibody was purchased from EMD Millipore, (Burlington, MA, USA, cat# ST1202).

RNA-sequencing

Total RNA was isolated by homogenizing 25–30 mg gastrocnemius tissue with a handheld homogenizer in a solution containing Qiazol Lysis Reagent (Qiagen, Hilden, GER, cat# 79306). The RNA was separated and precipitated using chloroform and isopropanol. Extracted RNA was washed with ethanol then suspended in nuclease-free water. RNA concentration was determined using the EPOCH (Take3, BioTek, Winooski, VT, USA) spectrophotometer. RNA isolated from gastrocnemius underwent DNase digestion using TURBO™ DNase (ThermoFisher, Waltham, MA, USA, cat# AM2238) and was purified using RNA Clean and Concentrator 5 Columns (Zymo Research, Irvine, CA, USA, cat# R1014). Libraries were prepared with Illumina Stranded Total RNA Library Prep Ribo-Zero Gold Plus (Genome Builds mm10, M_musculus_Dec_2011, GRCm38) and RNA was sequenced using Illumina NovaSeq S4 Reagent Kit v1.5 150×150 bp Sequencing. Differentially expressed genes were identified using a 5% false discovery rate with DESeq2 version 1.30.00 and the hciR package. Data can be found on the Gene Expression Omnibus GSE167462. Hallmark pathways were identified using the fast gene set enrichment analysis in MSigDB using a 10% FDR. Pathways significantly altered and overlapping between contrasts were chosen for presentation in the results section. The top gene changes reversed by MET+LEU were identified by finding the highest altered genes due to HU, that had the highest change in the opposite direction due to MET+LEU.

Statistical Analysis

Data are reported as means ± SE with individual data points displayed. To determine the main effects of the treatments on HU and reloading and their interactions, a two-way ANOVA was utilized and Sídák's post-hoc analysis was used to determine differences within independent treatments. For comparing AMB vs. HU (with different conditions) unpaired sample t-tests were performed. Normality was tested for each data set utilizing Shapiro-Wilk tests and Q-Q plots. For all statistical comparisons, significance was set at the level of $p<0.05$. All analysis and figures were conducted with Graph Pad Prism 9 (La Jolla, CA, USA).

Results

Body Mass and Muscle Morphological Characteristics

Body mass, soleus and gastrocnemius mass and myofiber cross sectional area (CSA) were unaltered by MET+LEU, MET or LEU treatment during HU or Recovery (Figure 1b–p), with the exception of MET increasing gastrocnemius CSA compared to Vehicle at 7d RL ($p=0.015$; Figure 1l). During HU, Vehicle, MET+LEU, and LEU decreased body mass compared to AMB ($p=0.028$, $p=0.010$, $p=0.006$; Figure 1b–d). During HU, Vehicle, MET+LEU, MET, and LEU decreased gastrocnemius mass compared to AMB ($p<0.001$,

$p<0.001$, $p<0.001$, $p<0.001$; Figure 1e–g). During HU, Vehicle, MET+LEU, MET, and LEU decreased soleus mass compared to AMB ($p<0.001$, $p<0.001$, $p<0.001$, $p<0.001$; Figure 1h–j). During HU, Vehicle, MET+LEU, MET and LEU decreased gastrocnemius CSA compared to AMB ($p<0.001$, $p<0.001$, $p<0.001$, $p<0.001$; Figure 1k–m). During HU, Vehicle, MET+LEU, MET, and LEU decreased soleus CSA compared to AMB ($p=0.008$, $p=0.002$, $p=0.010$, $p=0.043$; Figure 1n–p).

Whole Body Strength and Muscle Force

During HU, Vehicle, MET, and LEU (but not MET+LEU) decreased whole body grip strength compared to AMB ($p=0.026$, $p=0.015$, $p=0.012$; Figure 2a–c). During HU, MET+LEU strongly trended to increased whole body grip strength compared to Vehicle ($p=0.052$; Figure 2a). In contrast, MET or LEU did not affect whole body grip strength compared to Vehicle during HU and reloading (7 and 14d) (Figure 2b–c).

During HU, soleus ex vivo isometric specific force was decreased in Vehicle (but not MET+LEU) compared to AMB at 60 and 80 Hz ($p=0.037$, $p=0.042$; Figure 2d–f) and was increased with MET+LEU compared to Vehicle at 60, 80, 100, 125, 150 and 200 Hz ($p=0.007$, $p=0.006$, $p=0.008$, $p=0.012$, $p=0.013$, $p=0.016$; Figure 2d). MET or LEU did not alter specific force production compared to Vehicle (Figure 2e–f). MET+LEU (but not MET or LEU) increased soleus absolute ex vivo isometric force production compared to Vehicle at the 100 Hz frequency (Figure 2g–i). MET+LEU (but not MET or LEU) also increased soleus isometric ex vivo specific and absolute force production at optimal length during a single pulse ($p=0.026$; Figure 2j, Figure 2k–o). Neither of the treatments (vs Vehicle) during reloading (7 and 14d), improved soleus specific force (Supplementary Figure 1a–f).

Myofiber Composition

During HU, gastrocnemius myosin heavy chain (MHC) type I fibers were increased in MET compared to AMB ($p=0.006$; Supplementary Figure 2b) and strongly trended to increase in LEU compared to AMB ($p=0.058$; Supplementary Figure 2c). During HU, gastrocnemius MHC IIa fibers were increased in MET and LEU compared to AMB ($p=0.002$, $p=0.031$; Supplementary Figure 2e and f). Gastrocnemius MHC type IIa fibers were decreased at 14d RL in MET+LEU and LEU compared to Vehicle ($p=0.004$, $p=0.015$; Supplementary Figure 2d and f). During HU, gastrocnemius MHC type IIx fibers increased in Vehicle and MET compared to AMB ($p=0.007$, $p=0.005$; Supplementary Figures 2g–i). At 7d RL, MET had decreased gastrocnemius MHC type IIx fibers compared to Vehicle ($p=0.019$, Supplementary Figure 2h) which increased compared to Vehicle by 14d RL ($p=0.012$; Supplementary Figure 2h). During HU, gastrocnemius MHC type IIb fibers were decreased in Vehicle, MET, and LEU (but not MET+LEU) compared to AMB ($p=0.030$, $p=0.001$, $p=0.047$; Supplementary Figures 2j–l). At 14d RL, gastrocnemius MHC type IIb fibers decreased with MET compared to Vehicle ($p=0.012$; Supplementary Figure 2k).

Soleus MHC type IIa fibers at 14d RL were decreased in MET compared to Vehicle ($p=0.014$; Supplementary Figure 2q). During HU, soleus MHC hybrid type I/IIa fibers were decreased in Vehicle and MET, and strongly trended to decrease in MET+LEU compared to AMB ($p=0.016$, $p=0.033$, $p=0.053$; Supplementary Figure 2s–u). Soleus MHC hybrid type

I/IIa fibers at 7d RL were decreased in MET+LEU and LEU compared to Vehicle (p=0.022, p=0.039; Supplementary Figure 2s and u). Soleus MHC hybrid type I/IIa fibers at 14d RL were decreased in MET compared to Vehicle (p=0.043; Supplementary Figure 2t). During HU, soleus MHC type IIx fibers were increased in Vehicle and MET+LEU and strongly trended to increase in LEU compared to AMB (p=0.009, p=0.007, p=0.050; Supplementary Figure 2v–x). Soleus MHC type IIx fibers were increased at 14dRL in MET compared to Vehicle (p=0.001; Supplementary Figure 2w).

Satellite Cells, Central Nuclei, and Immunoglobin G

MET+LEU increased gastrocnemius satellite cells during HU compared to Vehicle (p=0.027; Figure 3a). During HU, MET strongly trended to decrease satellite cells compared to AMB (p=0.052; Figure 3b). MET increased gastrocnemius satellite cells at 7d RL (p=0.010), and decreased satellite cells at 14d RL compared to Vehicle (p=0.011; Figure 3b). LEU increased gastrocnemius satellite cells during HU (p=0.010) and 7d RL compared to Vehicle (p<0.001; Figure 3c). MET+LEU increased central nuclei throughout the intervention (HU and reloading) (main effect of treatment; p=0.013) and strongly trended to increase gastrocnemius central nuclei specifically at 7d RL compared to Vehicle (p=0.051, Figure 3d). MET did not alter gastrocnemius central nuclei compared to Vehicle during HU or reloading (7 and 14d) (Figure 3e), LEU treatment increased gastrocnemius central nuclei throughout the intervention (main effect of treatment; p=0.008, Figure 3f).

Neither treatment influenced soleus satellite cell abundance compared to Vehicle (Figure 3g–i). MET+LEU or MET did not affect soleus central nuclei content (Figure 3j–k). On the other hand, LEU increased soleus central nuclei content at 14d RL compared to Vehicle (p=0.038; Figure 3l). Representative images of gastrocnemius satellite cell and central nuclei content are displayed in Figure 3m–n.

During HU, muscle damage observed via immunoglobin G (IgG) content was not altered by Vehicle, MET+LEU, MET, or LEU compared to AMB (Supplementary Figure 3a–c). At 7d RL, MET+LEU decreased IgG content compared to Vehicle (p=0.039; Supplementary Figure 3a). Representative images of gastrocnemius IgG are displayed in Supplementary Figure 3d. Embryonic MHC staining was performed but not detected at any of the timepoints observed (data not shown).

Collagen Deposition and Turnover

During HU, Vehicle, MET+LEU, MET, and LEU increased gastrocnemius Sirius Red content compared to AMB (p=0.002, p<0.001, p=0.002, p<0.001; Figure 4a–c). MET+LEU decreased gastrocnemius Sirius Red content throughout the intervention (HU and reloading) (main effect of treatment; p=0.034) and during HU strongly trended to decrease Sirius Red content compared to Vehicle (p=0.052; Figure 4a). MET decreased Sirius Red content throughout the intervention compared to Vehicle (main effect of treatment; p=0.032; Figure 4b). LEU did not alter gastrocnemius Sirius Red content compared to Vehicle (Figure 4c). MET+LEU increased gastrocnemius B-CHP: Collagen IV ratio, a surrogate marker for collagen turnover, during reloading (7 and 14d) compared to Vehicle (p=0.027 and <0.001 respectively, Figure 4d). The MET+LEU-induced collagen turnover increase was driven by

decreased collagen IV content (main effect of treatment; p=0.001) as B-CHP did not change with treatments (Supplementary Figure 4a and d). Compared to AMB, gastrocnemius B-CHP increased during HU in Vehicle and MET (p=0.029, p=0.043; Supplementary Figure 4a–c). During HU, MET trended to increase gastrocnemius collagen turnover (p=0.058) and increased collagen turnover at 14d RL compared to Vehicle (p=0.021, Figure 4e), an effect also driven by decreased collagen IV during HU (p=0.033), with no MET-induced change in B-CHP (Supplementary Figure 4b and e). LEU did not alter gastrocnemius collagen turnover compared to Vehicle (Figure 4f), with no effect on collagen IV or B-CHP (Supplementary Figure 4c and f).

During HU, Vehicle, MET+LEU, MET, and LEU increased soleus Sirius Red content compared to AMB (p=0.002, p=0.004, p=0.043, p=0.003; Figure 4g–h). Neither MET nor MET+LEU altered soleus Sirius Red content compared to Vehicle at any timepoint (Figure 4g–h), LEU increased soleus Sirius Red content compared to Vehicle at 7d RL (p=0.004; Figure 4i). Neither treatment altered soleus collagen turnover compared to Vehicle (Figure 4j–l). Neither MET nor MET+LEU treatment altered soleus B-CHP compared to Vehicle yet, LEU increased soleus B-CHP at 14d RL (p=0.002; Supplementary Figure 4g–i). During HU, LEU increased soleus B-CHP compared to AMB (p=0.018; Supplementary Figure 4i). Neither MET+LEU nor MET treatment affected soleus collagen IV content (Supplementary Figure 4j–k). LEU increased soleus collagen IV content throughout the intervention compared to Vehicle (main effect of treatment; p=0.010; Supplementary Figure 4l) and during HU increased soleus collagen IV content compared to AMB (p=0.002; Supplementary Figure 4l). Representative images of gastrocnemius Sirius Red, B-CHP, and collagen IV are found in Figure 4m.

AMPKα and mTORC1 Signaling

Neither treatment altered gastrocnemius AMPKα (Thr172), acetyl-CoA carboxylase (ACC Ser79), or total PGC-1α protein levels compared to Vehicle during the intervention time course (Figure 5a–i). Similarly, neither treatment altered gastrocnemius mTORC1 (Ser2448), 70 kDa ribosomal protein S6 kinase (p70S6K Thr389), or ribosomal protein S6 (rpS6 Ser240/244) levels during HU, 7 or 14d RL compared to Vehicle (Figure 5j–r). Representative immunoblots for AMPKα and mTORC1 signaling are reported in Figure 5s and t, respectively. During HU, gastrocnemius phosphorylated rpS6 Ser240/244 levels were decreased compared to AMB in Vehicle, MET+LEU, MET and LEU (p=0.001, p=0.003, p=0.002, p<0.001; Figure 5p–r).

RNA-sequencing

Gene Set Enrichment Analysis (GSEA) identified Hallmark Pathways altered by MET+LEU in gastrocnemius during HU, 7 and 14d RL are reported in Figure 6a. Vehicle, MET, and LEU independent effects on the pathways are also displayed in Figure 6a. During HU, inflammation, hypoxia, and apoptosis related pathways (Inflammatory Response, Interferon Gamma Response, TNFα Signaling Via NF-κB, Hypoxia, and Apoptosis) were increased by HU (AMB vs. Veh) and reduced with MET+LEU treatment while Myogenesis, Notch Signaling, and Oxidative Phosphorylation pathways were increased in MET+LEU compared to Vehicle. During HU, LEU reduced inflammation and apoptosis

related pathways, MET reduced Myogenesis and Oxidative Phosphorylation and enhanced inflammatory and apoptosis pathways compared to Vehicle. The Myogenesis pathway was elevated at 7d RL in all treatments compared to Vehicle. At 7d RL, MET and LEU reduced Oxidative Phosphorylation pathway compared to Vehicle, but not in the case for MET+LEU. At 14d RL, pathways related to inflammation (Inflammatory Response and Interferon Gamma Response) were increased with all treatments. Due to an increase in Oxidative Phosphorylation pathway during HU with MET+LEU, we followed up with total citrate synthase and mitochondrial complex protein analysis. Total citrate synthase and mitochondrial complex proteins were not altered with MET+LEU compared to Vehicle during HU (Supplementary Figure 5a–g).

A list of the top gene changes induced by HU and reloading of aged mice, and altered by MET+LEU, can be found in Figure 6b. MET and LEU influence on the genes are also displayed in Figure 5b. Regarding the top changed genes, Fosb, Fos, Dusp1, and Klf6 appeared within the inflammatory GSEA pathways in Vehicle compared to MET+LEU treated mice during HU.

Discussion

The primary finding in aged mice was that during disuse metformin and leucine combination (MET+LEU) (but not the individual treatments) resolved grip strength and soleus force production decrements and increased gastrocnemius satellite cell content while alleviating gastrocnemius collagen deposition. During recovery, MET+LEU improved gastrocnemius collagen remodeling. Secondly, MET+LEU treatment reversed muscle transcriptional programs disrupted by disuse such as inflammatory and myogenesis pathways and this was independent of mTORC1 and AMPKα cellular signaling. Together, these data suggest that during disuse MET+LEU enhanced satellite cell content and lowered fibrotic deposition. The muscle phenotype following the combined treatment may partly be related to the anti-inflammatory and myogenesis-promoting properties of the treatments.

A major finding from this study was that MET+LEU treatment increased satellite cell abundance in gastrocnemius during disuse with increased centralized nuclei (a marker of regenerated muscle) at recovery. This response was concomitant with an increased transcriptional program related to myogenesis during disuse. It is clear that satellite cells are critical for muscle regeneration following injury [21], but the role of satellite cells for muscle regrowth following disuse, at least in young mice, appears questionable [29]. Rather, the importance of satellite cells during disuse and recovery in aged muscle may be more evident. Aging muscle characteristically has lower satellite cell content and is further reduced after disuse [2], while aged muscle is more susceptible to disuse-induced damage. Thus, an overall lower muscle regenerative cell capacity combined with enhanced muscle injury after disuse may possibly contribute to poor muscle recovery in aging. We did observe increased central nuclei and reduced IgG with MET+LEU at 7d RL. Though speculative, it is possible that muscle injury occurred early in recovery (≤1–2 days) from disuse [34] and was alleviated at 7d RL as central nuclei are more present as IgG is cleared [35]. Consistent with this observed pro-regenerative treatment response, metformin alone has been shown to promote satellite cell accumulation during recovery from burn injury in young mice [6]

and, in another study, leucine independently was able to increase myogenic progenitor cell proliferation in vitro [20]. After dissecting the individual treatment effects, it appears that leucine was primarily responsible for the initial increase in satellite cells during disuse. However, at early recovery (7d), metformin treatment alone also increased satellite cell content. Therefore, metformin and leucine likely work synergistically to enhance satellite cell abundance during disuse in aged mice possibly through enhanced myogenesis.

Another major finding was that MET+LEU treatment alleviated gastrocnemius collagen accumulation (primarily collagen I and III) during disuse. Collagen IV, a primary basement membrane collagen, was also reduced during recovery with the combined treatment. Excessive muscle fibrosis is commonly observed in aged skeletal muscle and is associated with poor muscle regeneration [23] thus it was encouraging that the dual treatment was able to ameliorate the fibrotic condition in aged muscle. It is likely that metformin treatment alone contributed to the MET+LEU-mediated reduction in collagen especially in light that leucine treatment surprisingly resulted in the reverse response (increased collagen deposition). This is consistent with other studies in young adult rodents such that metformin was able to reduce fibrosis caused by high fat feeding [25] and limb immobilization [7]. Intramuscular fibroblasts are primarily responsible for collagen and ECM deposition in skeletal muscle. Due to the known coordination of fibroblasts and satellite cells [21, 22], it is possible that the MET+LEU-mediated accumulation of satellite cells may have promoted downstream regulation of collagen content. It is also important to point out that MET+LEU treatment may work in muscle types uniquely since gastrocnemius satellite cell and collagen accumulation was improved but not in soleus muscle. Recovery from disuse in aged rats has been observed to increase muscle collagen protein synthesis to a greater extent in fast-twitch tibialis anterior compared to the slow-twitch soleus [36]. Additionally, in aged rats, disuse caused greater deficits in denervation, ubiquitin, and autophagy markers in the tibialis anterior compared to soleus [37]. Therefore, MET+LEU treatment had preferential influence on the fast-twitch gastrocnemius possibly due to greater impairments in this muscle during disuse and recovery conditions compared to the soleus.

Loss of muscle strength and size due to disuse is well established to occur with aging in rodents and humans [1, 37]. We found that MET+LEU treatment alleviated whole body strength and soleus force loss during disuse and was independent of changes to muscle or fiber size. We were surprised that muscle or fiber size was not altered by the dual treatment, since metformin has previously been effective to ameliorate muscle atrophy caused by limb immobilization [7], high fat feeding [25] and burn injury [6]. Similarly, leucine is a potent stimulator of muscle protein synthesis [11] and, in combination with antioxidant cocktail, was able to prevent disuse-induced muscle atrophy in adult rats [13]. Though we used a similar dosage as in prior rodent studies, it may be possible that the severity of muscle atrophy caused by hindlimb unloading in aged mice may have been too excessive to overcome suggesting that there might be more room for optimizing dosages. A possible, yet simplistic explanation why MET+LEU treatment improved strength during disuse may be because of causing less collagen accumulation resulting in increased contractile tissue per cross sectional area of muscle mass thus overall improved muscle quality. We also cannot discount unknown positive effects of the combined treatment on the neuromuscular junction since muscle recovery following disuse in aged mice are characterized with suppressed

neuromuscular innervation [37]. We did not observe individual effects of metformin or leucine on muscle function during disuse or recovery. This is somewhat consistent in the human literature since metformin appears to hamper strength gains in healthy older adults after resistance exercise training [4] and leucine supplementation is only able to partially protect muscle mass and strength loss during bed rest in middle-aged adults [38]. Therefore, the combined effects of metformin and leucine may be needed to enhance muscle quality during disuse in aged mice but is unable to improve muscle size.

Little is known of the influence metformin and leucine has on fiber type during hindlimb unloading and reloading in aged mice. We observed in gastrocnemius and soleus that disuse resulted in increased MHC IIx fibers in Vehicle treated mice as slow-to-fast MHC transition commonly occurs with disuse [39]. Interestingly, we found a decrease in more oxidative MHC types and an increase in fast twitch (MHC IIx) in soleus and gastrocnemius at 14d RL with MET treatment. We also identified a decrease in gastrocnemius MHC IIa fibers with MET+LEU at 14d RL. However, metabolic GSEA pathways (glycolysis or fatty acid metabolism) at 14d RL were not altered with MET+LEU nor did we see changes in muscle function or size at this timepoint. Thus, it is likely that the modest fiber switching noted with MET+LEU treatment did not play a major role in the primary findings during disuse and recovery.

Metformin treatment is commonly associated with enhanced AMPKα activation [8] while leucine activates muscle mTORC1 signaling [11]. However, neither of these pathways were activated following the treatments. A consideration is that traditional immunoblotting was not sensitive enough to capture possible modest AMPKα and mTORC1 signaling responses since metformin and leucine were provided in drinking water and delivered incrementally throughout rodent drinking periods. It is also possible that metformin may work independent of AMPKα in muscle [40]. Therefore, to better comprehend the mechanisms of MET+LEU treatment, we conducted RNA-sequencing in gastrocnemius to gain insight on the global muscle transcriptome. A notable observation was that MET+LEU treatment increased pathways related to oxidative phosphorylation during disuse. Disuse and recovery result in mitochondrial dysfunction in aging muscle [41]. However, the transcriptional pathway changes were not in agreement with surrogate markers of total mitochondrial content suggesting that more extensive mitochondrial phenotyping may be necessary. Another interesting observation was that inflammation pathways were reduced by MET+LEU treatment during disuse. Inflammatory signaling is known to contribute to disuse-induced muscle atrophy and recovery in rodents [42] and associated with reduced strength in older adults [43]. Importantly, inflammatory responses (like during disuse and aging) are known to exacerbate myofibroblast activation, ECM remodeling and contribute to poor satellite cell function [44, 45]. Therefore, we surmise that MET+LEU treatment may have reduced inflammatory pathways resulting in lower collagen deposition and enhanced turnover, together promoting an improved extracellular niche for satellite cells to exist and function (Figure 7), but further investigation of this proposed mechanism is warranted.

In summary, MET+LEU treatment during muscle disuse resolved strength loss independent of muscle size and this outcome was further complimented by increased satellite cell content. MET+LEU treatment also promoted collagen remodeling during recovery.

MET+LEU treatment enriched muscle transcriptional pathways related to myogenesis and reduced inflammation that, together, may be related to improved muscle quality in aging muscle.

Supplementary Material

Refer to Web version on PubMed Central for supplementary material.

Acknowledgements

We would like to thank the Genomics and Cell Imaging Cores at the Health Sciences Center of the University of Utah. Figure 7 was partially created using BioRender.com. Funding for this project was provided by NIA Grant (R03AG064216) awarded to M.J.D and funding from the Ruth L. Kirschstein National Research Service Award NIH 1T32HL139451 (postdoctoral fellowship awarded to Z.S.M.). J.J.P. was supported from a University of Utah Sports Medicine Fellowship Grant.

Abbreviations

14d RL	14-day reloading
7d RL	7-day reloading
ACC	Acetyl-CoA carboxylase
AMB	Ambulatory baseline
AMPKα	AMP-activated protein kinase
B-CHP	Biotinylated-collagen hybridizing peptide
CSA	Cross sectional area
DAPI	4′,6-diamidino-2-phenylindole
ECM	Extracellular matrix
GSEA	Gene set enrichment analysis
HU	Hindlimb Unloading
IgG	Immunoglobin G
LEU	Leucine
MET	Metformin
MET+LEU	Metformin + Leucine combination
MHC	Myosin heavy chain
mTORC1	Mechanistic target of rapamycin complex 1
p70S6K	70 kDa ribosomal protein S6 kinase
PGC-1α	PPARG coactivator-1alpha

rpS6	Ribosomal protein S6
SIRT1	Sirtuin 1

References

1. Pisot R, et al.Greater loss in muscle mass and function but smaller metabolic alterations in older compared with younger men following 2 wk of bed rest and recovery. J Appl Physiol (1985). 2016;120(8):922–9. DOI: 10.1152/japplphysiol.00858.2015. [PubMed: 26823343]
2. Suetta C, et al.Ageing is associated with diminished muscle re-growth and myogenic precursor cell expansion early after immobility-induced atrophy in human skeletal muscle. J Physiol. 2013;591(15):3789–804. DOI: 10.1113/jphysiol.2013.257121. [PubMed: 23732643]
3. Brown CJ, et al.Exercise program implementation proves not feasible during acute care hospitalization. J Rehabil Res Dev. 2006;43(7):939–46. DOI: 10.1682/jrrd.2006.04.0034. [PubMed: 17436179]
4. Walton RG, et al.Metformin blunts muscle hypertrophy in response to progressive resistance exercise training in older adults: A randomized, double-blind, placebo-controlled, multicenter trial: The MASTERS trial. Aging Cell. 2019;18(6):e13039. DOI: 10.1111/acel.13039. [PubMed: 31557380]
5. Langone F, et al.Metformin protects skeletal muscle from cardiotoxin induced degeneration. PLoS One. 2014;9(12):e114018. DOI: 10.1371/journal.pone.0114018. [PubMed: 25461598]
6. Yousuf Y, et al.Metformin alleviates muscle wasting post-thermal injury by increasing Pax7-positive muscle progenitor cells. Stem Cell Res Ther. 2020;11(1):18. DOI: 10.1186/s13287-019-1480-x. [PubMed: 31915055]
7. Bosi PL, et al.Metformin Minimizes the Morphometric Alterations in the Soleus Muscle of Rats Submitted to Articular Immobilization. Rev Bras med Esporte. 2008;14(5):436–439. DOI: 10.1590/S1517-86922008000500007
8. Suwa M, et al.Metformin increases the PGC-1alpha protein and oxidative enzyme activities possibly via AMPK phosphorylation in skeletal muscle in vivo. J Appl Physiol (1985). 2006;101(6):1685–92. DOI: 10.1152/japplphysiol.00255.2006. [PubMed: 16902066]
9. Rivera ME, Lyon ES, and Vaughan RA. Effect of metformin on myotube BCAA catabolism. J Cell Biochem. 2020;121(1):816–827. DOI: 10.1002/jcb.29327. [PubMed: 31385363]
10. Dinulovic I, et al.PGC-1alpha modulates necrosis, inflammatory response, and fibrotic tissue formation in injured skeletal muscle. Skelet Muscle. 2016;6:38. DOI: 10.1186/s13395-016-0110-x. [PubMed: 27833743]
11. Drummond MJ and Rasmussen BB. Leucine-enriched nutrients and the regulation of mammalian target of rapamycin signalling and human skeletal muscle protein synthesis. Curr Opin Clin Nutr Metab Care. 2008;11(3):222–6. DOI: 10.1097/MCO.0b013e3282fa17fb. [PubMed: 18403916]
12. Combaret L, et al.A leucine-supplemented diet restores the defective postprandial inhibition of proteasome-dependent proteolysis in aged rat skeletal muscle. J Physiol. 2005;569(Pt 2):489–99. DOI: 10.1113/jphysiol.2005.098004. [PubMed: 16195315]
13. Savary-Auzeloux I, et al.A dietary supplementation with leucine and antioxidants is capable to accelerate muscle mass recovery after immobilization in adult rats. PLoS One. 2013;8(11):e81495. DOI: 10.1371/journal.pone.0081495. [PubMed: 24312309]
14. Backx EMP, et al.Leucine Supplementation Does Not Attenuate Skeletal Muscle Loss during Leg Immobilization in Healthy, Young Men. Nutrients. 2018;10(5) DOI: 10.3390/nu10050635.
15. English KL, et al.Leucine partially protects muscle mass and function during bed rest in middle-aged adults. Am J Clin Nutr. 2016;103(2):465–73. DOI: 10.3945/ajcn.115.112359. [PubMed: 26718415]
16. Amin SN, et al.Synergistic actions of vitamin D and metformin on skeletal muscles and insulin resistance of type 2 diabetic rats. J Cell Physiol. 2018;233(8):5768–5779. DOI: 10.1002/jcp.26300. [PubMed: 29205344]

17. Fu L, et al.Leucine amplifies the effects of metformin on insulin sensitivity and glycemic control in diet-induced obese mice. Metabolism. 2015;64(7):845–56. DOI: 10.1016/j.metabol.2015.03.007. [PubMed: 25858853]

18. Petrocelli JJ and Drummond MJ. PGC-1alpha-Targeted Therapeutic Approaches to Enhance Muscle Recovery in Aging. Int J Environ Res Public Health. 2020;17(22) DOI: 10.3390/ijerph17228650.

19. Csapo R, Gumpenberger M, and Wessner B. Skeletal Muscle Extracellular Matrix - What Do We Know About Its Composition, Regulation, and Physiological Roles? A Narrative Review. Front Physiol. 2020;11:253. DOI: 10.3389/fphys.2020.00253. [PubMed: 32265741]

20. Dai JM, et al.Leucine Promotes Proliferation and Differentiation of Primary Preterm Rat Satellite Cells in Part through mTORC1 Signaling Pathway. Nutrients. 2015;7(5):3387–400. DOI: 10.3390/nu7053387. [PubMed: 26007333]

21. Murphy MM, et al.Satellite cells, connective tissue fibroblasts and their interactions are crucial for muscle regeneration. Development. 2011;138(17):3625–37. DOI: 10.1242/dev.064162. [PubMed: 21828091]

22. Fry CS, et al.Myogenic Progenitor Cells Control Extracellular Matrix Production by Fibroblasts during Skeletal Muscle Hypertrophy. Cell Stem Cell. 2017;20(1):56–69. DOI: 10.1016/j.stem.2016.09.010. [PubMed: 27840022]

23. Grounds MDAge-associated changes in the response of skeletal muscle cells to exercise and regeneration. Ann N Y Acad Sci. 1998;854:78–91. DOI: 10.1111/j.1749-6632.1998.tb09894.x. [PubMed: 9928422]

24. Yoshimura A, et al.Cyclic muscle twitch contraction inhibits immobilization-induced muscle contracture and fibrosis in rats. Connect Tissue Res. 2017;58(5):487–495. DOI: 10.1080/03008207.2016.1257004. [PubMed: 27813681]

25. Hasan MM, et al.Beneficial effects of metformin on muscle atrophy induced by obesity in rats. J Cell Biochem. 2019;120(4):5677–5686. DOI: 10.1002/jcb.27852. [PubMed: 30320911]

26. Pereira MG, et al.Leucine supplementation improves skeletal muscle regeneration after cryolesion in rats. PLoS One. 2014;9(1):e85283. DOI: 10.1371/journal.pone.0085283. [PubMed: 24416379]

27. Reidy PT, et al.Aging impairs mouse skeletal muscle macrophage polarization and muscle-specific abundance during recovery from disuse. Am J Physiol Endocrinol Metab. 2019;317(1):E85–E98. DOI: 10.1152/ajpendo.00422.2018. [PubMed: 30964703]

28. Ferreira JA, Crissey JM, and Brown M. An alternant method to the traditional NASA hindlimb unloading model in mice. J Vis Exp. 2011(49) DOI: 10.3791/2467.

29. Jackson JR, et al.Satellite cell depletion does not inhibit adult skeletal muscle regrowth following unloading-induced atrophy. Am J Physiol Cell Physiol. 2012;303(8):C854–61. DOI: 10.1152/ajpcell.00207.2012. [PubMed: 22895262]

30. Ferrara PJ, et al.Hypothermia Decreases O2 Cost for Ex Vivo Contraction in Mouse Skeletal Muscle. Med Sci Sports Exerc. 2018;50(10):2015–2023. DOI: 10.1249/MSS.0000000000001673. [PubMed: 29787474]

31. Smith LR and Barton ER. SMASH - semi-automatic muscle analysis using segmentation of histology: a MATLAB application. Skelet Muscle. 2014;4:21. DOI: 10.1186/2044-5040-4-21. [PubMed: 25937889]

32. Schindelin J, et al.Fiji: an open-source platform for biological-image analysis. Nat Methods. 2012;9(7):676–82. DOI: 10.1038/nmeth.2019. [PubMed: 22743772]

33. Reidy PT, et al.Neuromuscular electrical stimulation and protein during bed rest increases CD11b(+) skeletal muscle macrophages but does not correspond to muscle size or insulin sensitivity. Appl Physiol Nutr Metab. 2020;45(11):1261–1269. DOI: 10.1139/apnm-2020-0064. [PubMed: 32470312]

34. Tidball JG and Wehling-Henricks M. Macrophages promote muscle membrane repair and muscle fibre growth and regeneration during modified muscle loading in mice in vivo. J Physiol. 2007;578(Pt 1):327–36. DOI: 10.1113/jphysiol.2006.118265. [PubMed: 17038433]

35. Welc SS, et al.Differential Effects of Myeloid Cell PPARdelta and IL-10 in Regulating Macrophage Recruitment, Phenotype, and Regeneration following Acute Muscle Injury. J Immunol. 2020;205(6):1664–1677. DOI: 10.4049/jimmunol.2000247. [PubMed: 32817369]

36. Miller BF, et al.Muscle-specific changes in protein synthesis with aging and reloading after disuse atrophy. J Cachexia Sarcopenia Muscle. 2019;10(6):1195–1209. DOI: 10.1002/jcsm.12470. [PubMed: 31313502]

37. Baehr LM, et al.Age-related deficits in skeletal muscle recovery following disuse are associated with neuromuscular junction instability and ER stress, not impaired protein synthesis. Aging (Albany NY). 2016;8(1):127–46. DOI: 10.18632/aging.100879. [PubMed: 26826670]

38. Mobley CB, et al.Effects of Whey, Soy or Leucine Supplementation with 12 Weeks of Resistance Training on Strength, Body Composition, and Skeletal Muscle and Adipose Tissue Histological Attributes in College-Aged Males. Nutrients. 2017;9(9) DOI: 10.3390/nu9090972.

39. Schiaffino S and Reggiani C. Fiber types in mammalian skeletal muscles. Physiol Rev. 2011;91(4):1447–531. DOI: 10.1152/physrev.00031.2010. [PubMed: 22013216]

40. Turban S, et al.Defining the contribution of AMP-activated protein kinase (AMPK) and protein kinase C (PKC) in regulation of glucose uptake by metformin in skeletal muscle cells. J Biol Chem. 2012;287(24):20088–99. DOI: 10.1074/jbc.M111.330746. [PubMed: 22511782]

41. Trevino MB, et al.Loss of mitochondrial energetics is associated with poor recovery of muscle function but not mass following disuse atrophy. Am J Physiol Endocrinol Metab. 2019;317(5):E899–E910. DOI: 10.1152/ajpendo.00161.2019. [PubMed: 31479303]

42. Kwon OS, et al.MyD88 regulates physical inactivity-induced skeletal muscle inflammation, ceramide biosynthesis signaling, and glucose intolerance. Am J Physiol Endocrinol Metab. 2015;309(1):E11–21. DOI: 10.1152/ajpendo.00124.2015. [PubMed: 25968578]

43. Tuttle CSL, Thang LAN, and Maier AB. Markers of inflammation and their association with muscle strength and mass: A systematic review and meta-analysis. Ageing Res Rev. 2020;64:101185. DOI: 10.1016/j.arr.2020.101185. [PubMed: 32992047]

44. Alameddine HS and Morgan JE. Matrix Metalloproteinases and Tissue Inhibitor of Metalloproteinases in Inflammation and Fibrosis of Skeletal Muscles. J Neuromuscul Dis. 2016;3(4):455–473. DOI: 10.3233/JND-160183. [PubMed: 27911334]

45. Perandini LA, et al.Chronic inflammation in skeletal muscle impairs satellite cells function during regeneration: can physical exercise restore the satellite cell niche?FEBS J. 2018;285(11):1973–1984. DOI: 10.1111/febs.14417. [PubMed: 29473995]

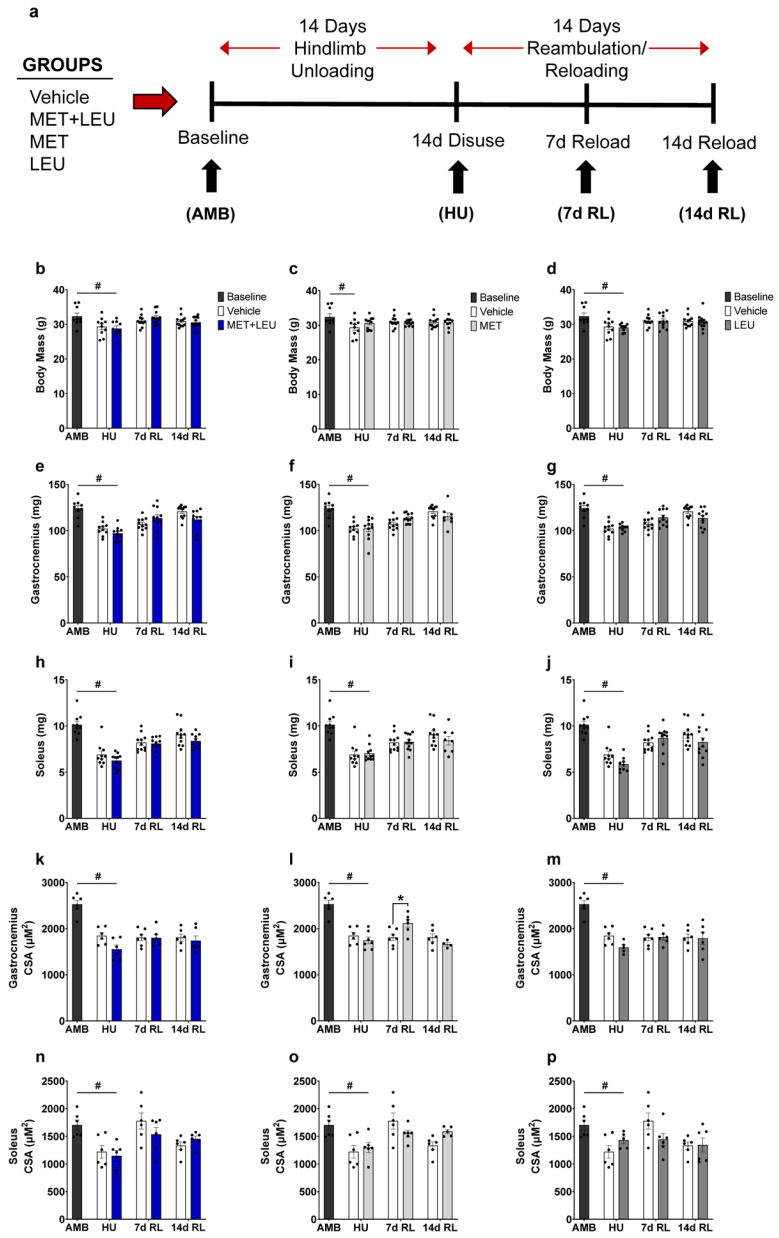

Fig. 1.

Experimental design schematic, body mass, and muscle morphological characteristics. (**a**) Four treatment groups (Vehicle control, MET+LEU, MET, and LEU) underwent 14 days of hindlimb unloading followed by 14 days of reambulation/reloading. Black arrows indicate the timepoints at which mice from each group were sacrificed. Age-matched ambulatory baseline (AMB) mice were not given MET+LEU, MET, or LEU and were collected as a baseline reference. Drinking water containing treatments or not (Vehicle control) began on the first day of HU and continued throughout experimentation. (**b-d**) Body mass in AMB, Vehicle, MET+LEU, MET and LEU. (**e-g**) Gastrocnemius mass in AMB, Vehicle, MET+LEU, MET and LEU. (**h-j**) Soleus mass in AMB, Vehicle, MET+LEU, MET and LEU. (**k-m**) Gastrocnemius cross sectional area (CSA) in AMB, Vehicle, MET+LEU, MET

and LEU. (**n-p**) Soleus CSA in AMB, Vehicle, MET+LEU, MET and LEU.). # $p<0.05$ vs. AMB, * $p<0.05$ vs. Vehicle. N=9–14/group for body and tissue mass, N=4–7/group for CSA measures.

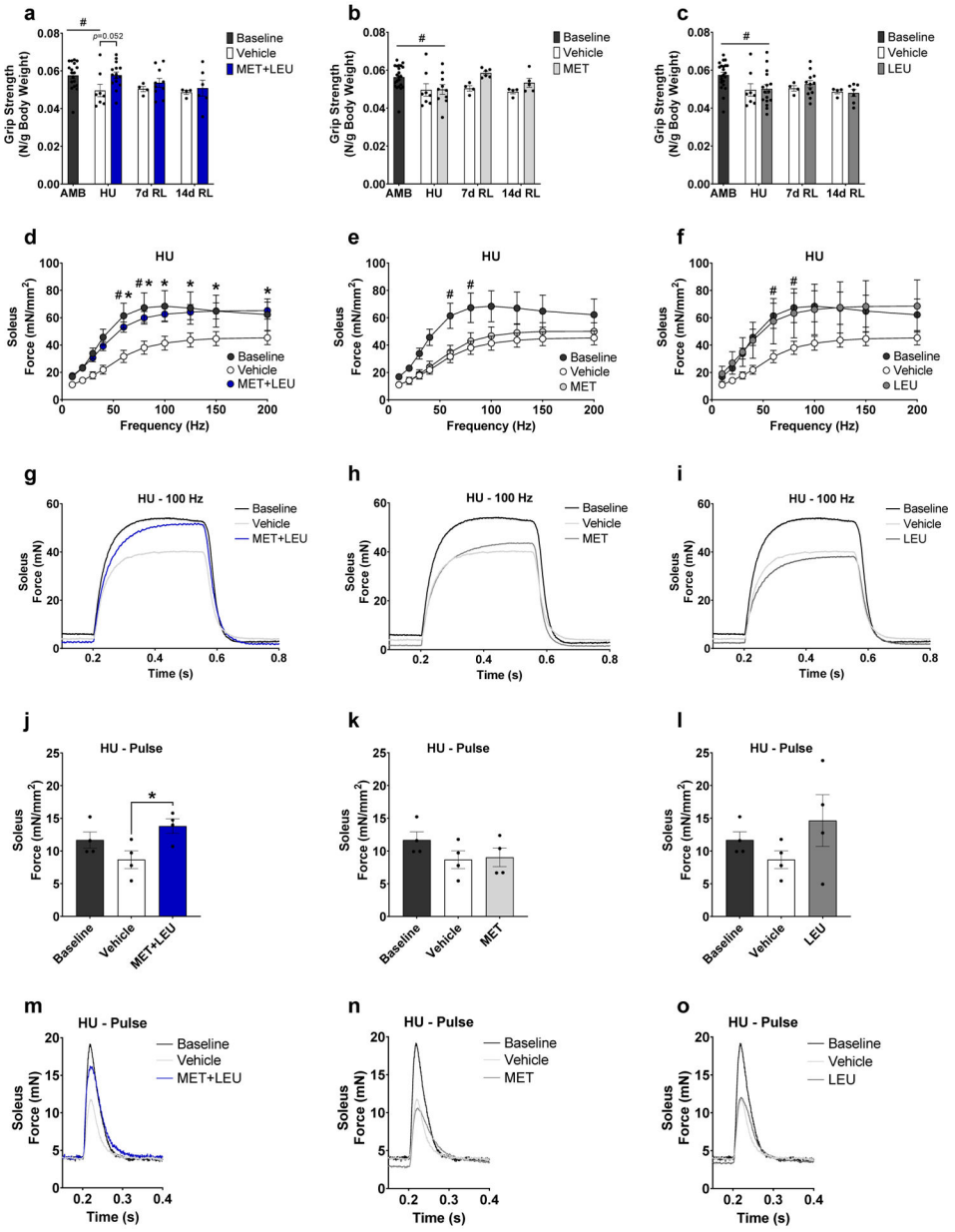

Fig. 2.

Whole body grip strength and soleus force production. (**a-c**) Whole body grip strength relative to body mass in MET+LEU, MET and LEU compared to Vehicle during HU and reloading (7 and 14d). (**d-f**) Soleus muscle ex vivo isometric specific force frequency curve in AMB, Vehicle, MET+LEU, MET and LEU during hindlimb unloading. (**g-i**) Absolute force contraction-relaxation at 100 Hz frequency in soleus of AMB, Vehicle, MET+LEU, MET and LEU during hindlimb unloading. (**j-l**) Specific force production during pulse (1 Hz) in soleus in AMB, Vehicle, MET+LEU, MET and LEU during hindlimb unloading. (**m-o**) Absolute soleus force contraction-relaxation during pulse (1 Hz). # $p<0.05$ vs. AMB, * $p<0.05$ vs. Vehicle. N=4–18/group, for force measurements N=4–6/group.

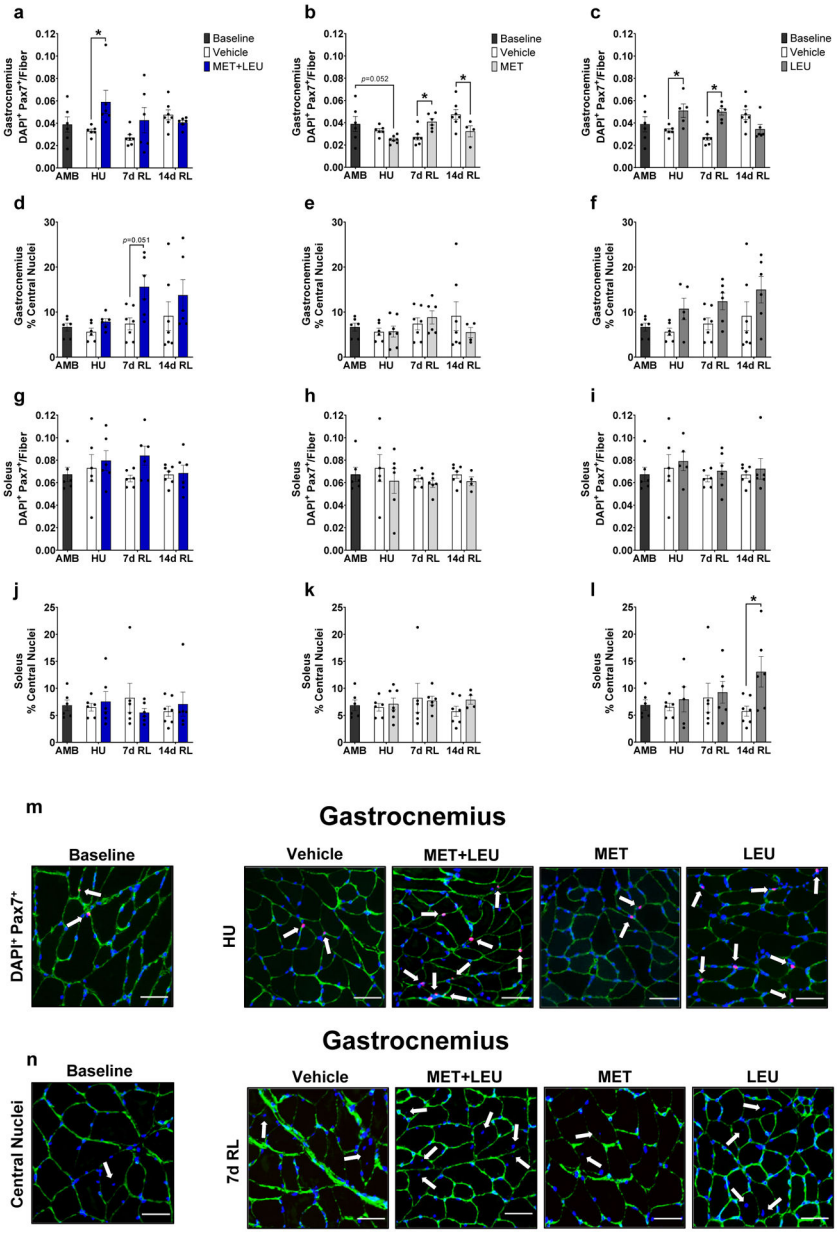

Fig. 3.

Gastrocnemius and soleus satellite cells and central nuclei. (**a-c**) Gastrocnemius satellite cells determined by $DAPI^+$ and $Pax7^+$ cells within the extracellular niche in AMB, Vehicle, MET+LEU, MET and LEU. (**d-f**) Gastrocnemius percentage of central nuclei in AMB, Vehicle, MET+LEU, MET and LEU. (**g-i**) Soleus satellite cells determined by $DAPI^+$ and $Pax7^+$ cells within the extracellular niche in AMB, Vehicle, MET+LEU, MET and LEU. (**j-l**) Soleus percentage of central nuclei in AMB, Vehicle, MET+LEU, MET and LEU. (**m**) Representative images of gastrocnemius satellite cells during HU with AMB, Vehicle, MET+LEU, MET and LEU. White arrows denote $DAPI^+$ and $Pax7^+$ cells within the extracellular niche. (**n**) Representative images of gastrocnemius central nuclei at 7d RL in

AMB, Vehicle, MET+LEU, MET and LEU. White arrows denote central nuclei. Scale bar for representative images is 50 μm. # $p<0.05$ vs. AMB, * $p<0.05$ vs. Vehicle. N=4–7/group.

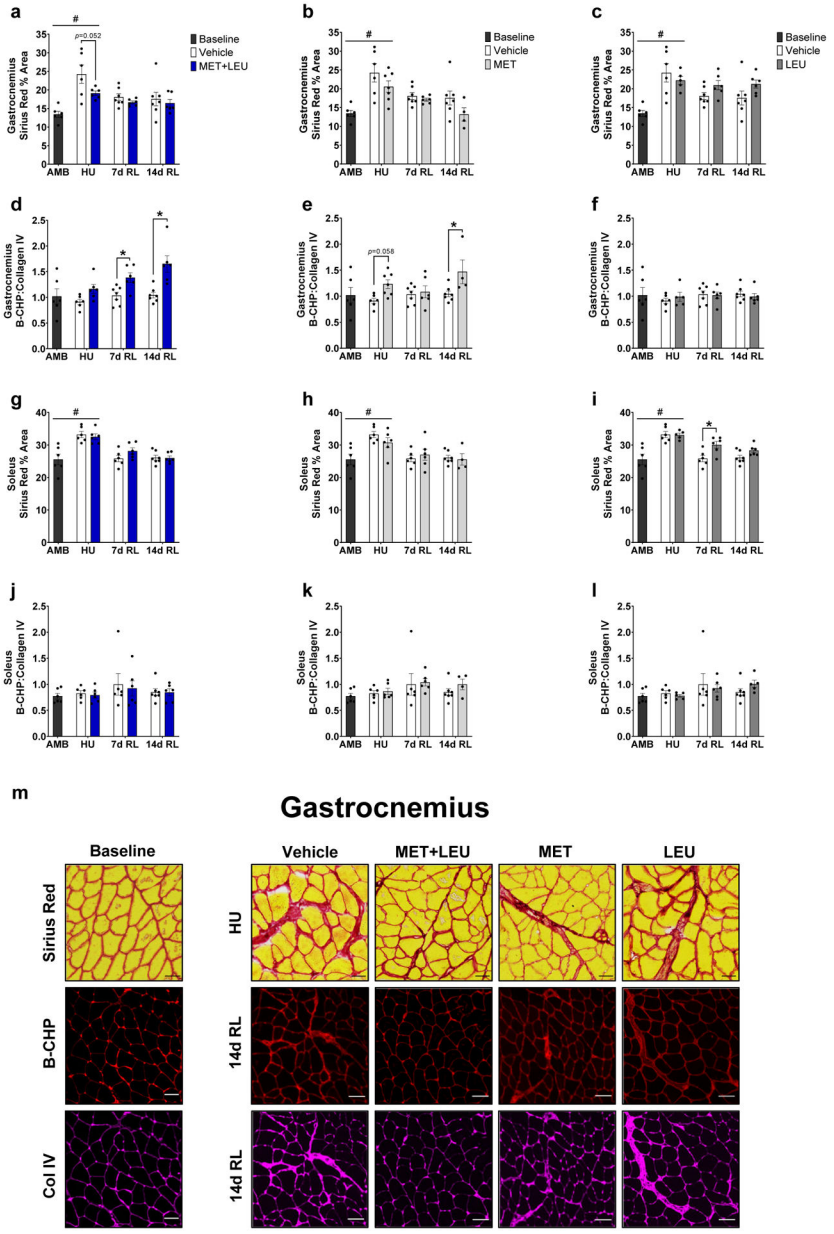

Fig. 4.

Gastrocnemius and soleus extracellular matrix deposition and turnover. (**a-c**) Gastrocnemius Sirius Red percent area in AMB, Vehicle, MET+LEU, MET and LEU. (**d-f**) Gastrocnemius B-CHP: Collagen IV ratio in AMB, Vehicle, MET+LEU, MET and LEU. (**g-i**) Soleus Sirius Red percent area in AMB, Vehicle, MET+LEU, MET and LEU. (**j-l**) Soleus B-CHP: Collagen IV ratio in AMB, Vehicle, MET+LEU, MET and LEU. (**m**) Representative images of gastrocnemius Sirius Red during HU and B-CHP and collagen IV at 14d RL with AMB, Vehicle, MET+LEU, MET and LEU. Scale bar for Sirius Red is 100 μM and 50 μM for B-CHP and collagen IV. # $p<0.05$ vs. AMB, * $p<0.05$ vs. Vehicle. N=4–7/group.

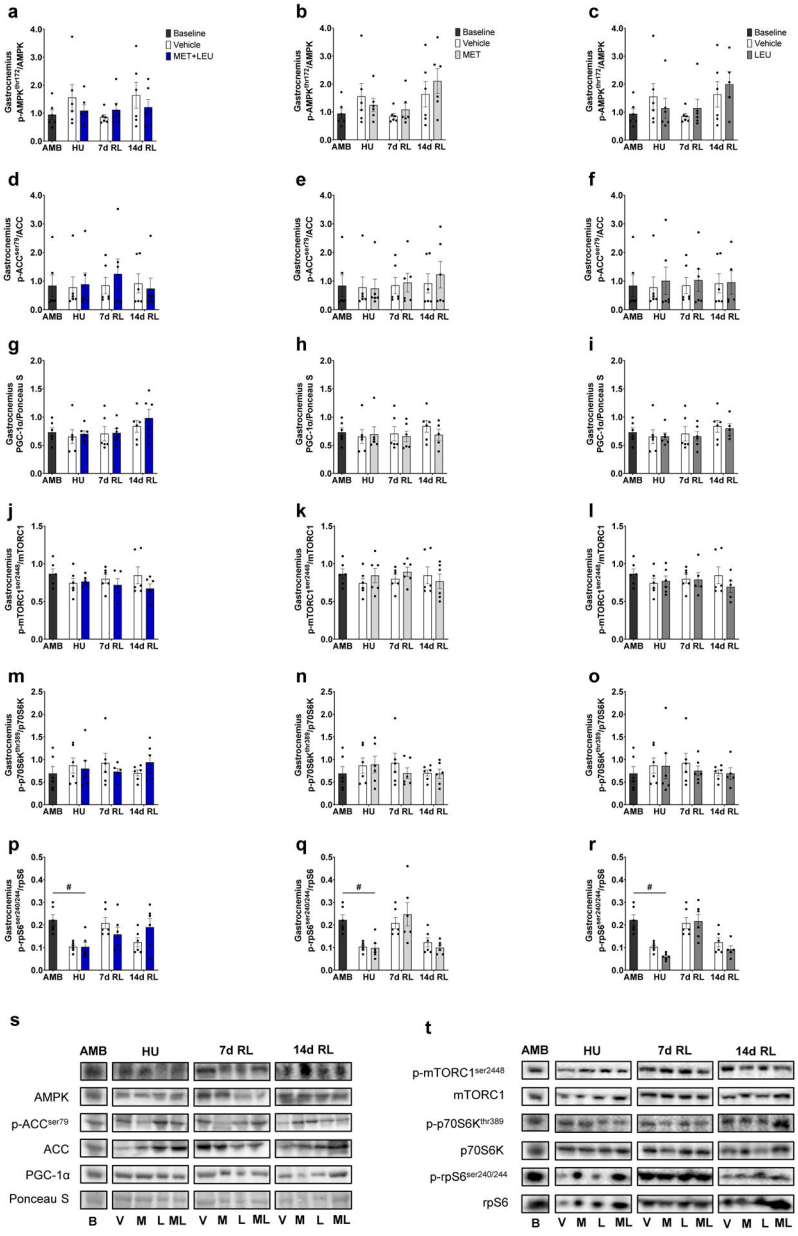

Fig. 5.

Gastrocnemius AMPKα and mTORC1 signaling. (**a-c**) Phosphorylated AMPKα threonine 172: total AMPK ratio in AMB, Vehicle, MET+LEU, MET and LEU. (**d-f**) Phosphorylated ACC serine 79: total ACC ratio in AMB, Vehicle, MET+LEU, MET and LEU. (**g-i**) Total PGC-1α: total protein determined by Ponceau S staining in AMB, Vehicle, MET+LEU, MET and LEU. (**j-l**) Phosphorylated mTOR serine 2448: total mTOR ratio in AMB, Vehicle, MET+LEU, MET and LEU. (**m-o**) Phosphorylated p70S6K threonine 389: total p70S6K ratio in AMB, Vehicle, MET+LEU, MET and LEU. (**p-r**) Phosphorylated rpS6 serine 240/244: total rpS6 ratio in AMB, Vehicle, MET+LEU, MET and LEU. (**s**) Representative immunoblots of AMPKα signaling. (**t**) Representative immunoblots of mTORC1 signaling. # $p<0.05$ vs. AMB. N=6/group.

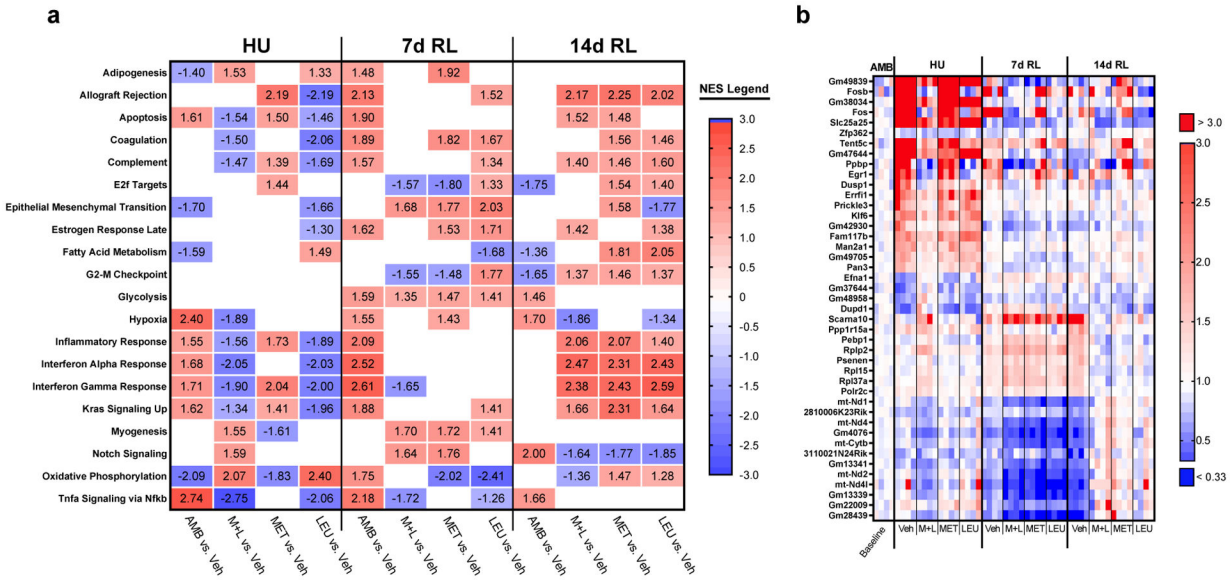

Fig. 6.

Gastrocnemius RNA-sequencing. (**a**) Top significantly impacted GSEA hallmark pathways altered by HU in Vehicle compared to AMB and rescued by MET+LEU during hindlimb unloading and reloading, MET and LEU individual effects presented. (**b**) Top individual genes altered by HU in Vehicle compared to AMB and rescued by MET+LEU during hindlimb unloading and reloading with MET and LEU individual effects presented. Significant pathways were determined by adjusted $p<0.05$. NES = Normalized enrichment scores. N=4/group.

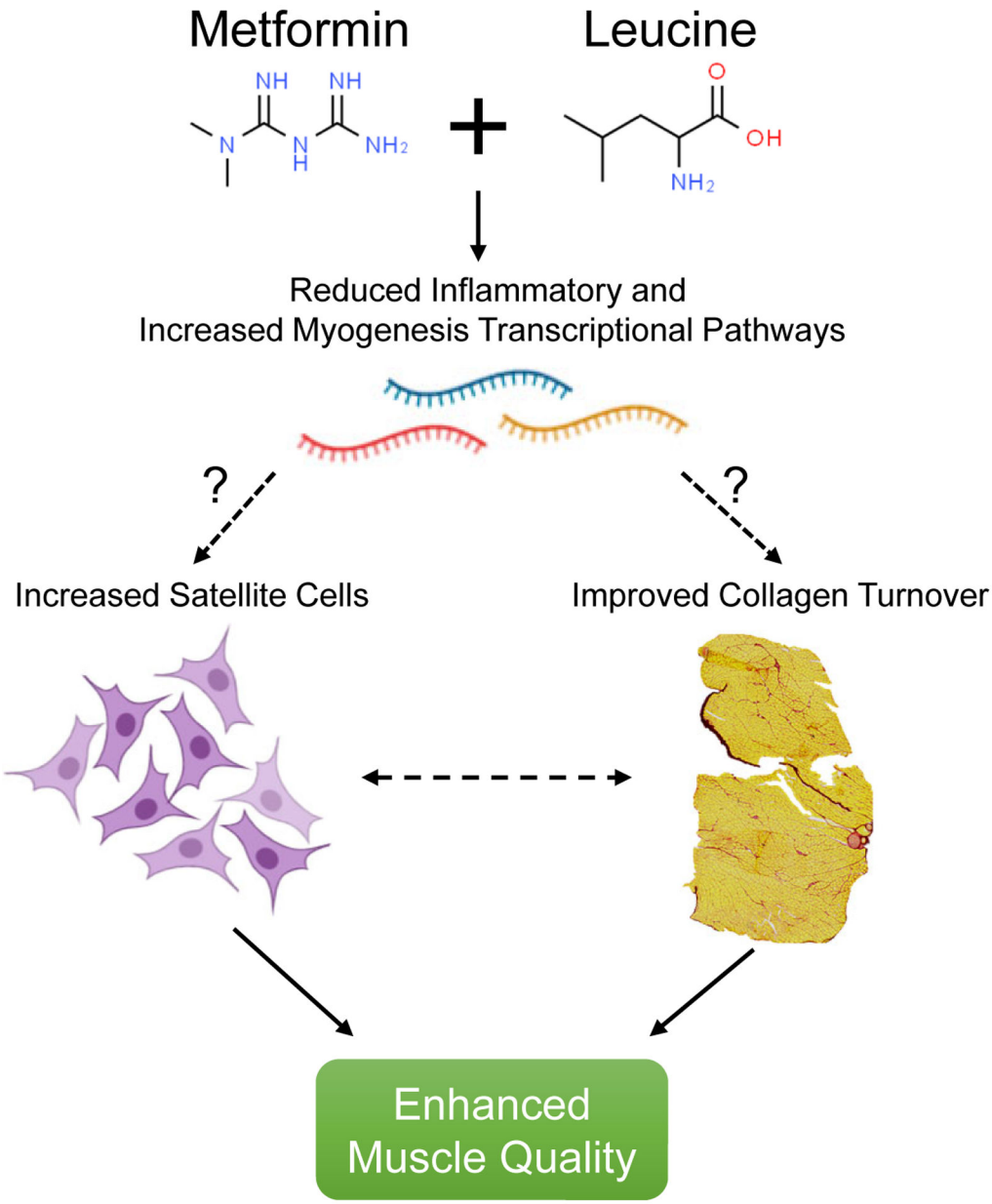

Fig. 7.

Proposed schematic of MET+LEU effects on muscle quality. MET+LEU resulted in reduced inflammatory and increased myogenesis transcriptomes. It is known that these pathways can directly influence satellite cell content and collage/extracellular matrix (ECM) deposition and turnover. We displayed an increase in satellite cells and collagen turnover with MET+LEU that was related to enhanced muscle quality in aged mice.